NUMERICAL INVESTIGATION OF ENTROPY GENERATION ANALYSIS DUE TO GRAPHENE OXIDE NANOFLUIDS FLOW THROUGH INCLINED CHANNEL

JAGADEESHWAR PASHIKANTI [*,1], SANTHOSH THOTA [1], NARASIMHULU DUNNA[2]
SUSMITHA PRIYADHARSHINI[1] D R

[1]*Department of Science and Humanities, Indian Institute of Information Technology Tiruchirappalli Tamil Nadu 620012, India.*

[2]*Department of Statistics and Applied Mathematics, School of Mathematics and Computer Sciences, Central University of Tamil Nadu 610005, India*

Studies on thermal radiation in nanofluid flow is crucial for the efficient use of their remarkable thermophysical properties and wide range of industrial uses. Besides the advantages of nanofluids on the whole, the nanoparticles dispersed in the fluids greatly influences the behaviour of the nanofluids. For instance, nanoparticles of magnetite, copper and graphene are significantly used in medical field for diagnosis and therapy. In view of these properties, graphene nanoparticles are the best choice for an enhanced thermal performance, as they significantly improve the performance of fluids in devices such as radiators and heat exchangers when dispersed either as nanoparticles or hybrid nanoparticles. Particularly, in channels, the nanofluid flow has wide applications including medicine such as the stenosis treatment. This investigation is one such computational study which considers the varying properties of the fluid flow between two inclined plates due to graphene oxide nanofluids. The flow is modelled considering the thermophoretic diffusion and Brownian motion. Spectral method is used to solve the complex coupled nonlinear equations under convective conditions. A comparison table shows agreement between literature and the obtained values. Also, the results obtained are graphed and discussed in detail along with entropy generation.

Keywords: entropy generation; velocity slip; graphene oxide nanofluids;

1. INTRODUCTION

The drawbacks of microfluids and viscous fluids such as the erosion of flow channels, clogging and deposition can be overcome by the nanofluids. While modelling their flow, thermophoretic diffusion and Brownian motion are considered for their significance in heat and mass transfer. Besides the advantages of nanofluids on the whole, the nanoparticles dispersed in the fluids greatly influences the behaviour of the nanofluids and nanoparticles of magnetite, copper and graphene are significantly used in medical field for diagnosis and therapy [1, 2]. In view of the thermophysical properties, graphene nanoparticles are the best choice for an enhanced thermal performance. They significantly improve the performance of fluids in devices such as radiators and heat exchangers when dispersed either as nanoparticles or hybrid nanoparticles. [3-6]

Extensive applications of thermal radiation and chemical reaction in different propulsion systems, atomic plants, turbines, manufacturing of polymers, fertilizers and dyes etc. signifies its importance in Computational Fluid Dynamics. Noteworthy investigations such as the study by Srinivasacharya and Ayano [7], investigated the impacts of chemical reaction on a micropolar fluid with MHD and cross-diffusion effects with a conclusion that the microrotation, concentration and velocity profiles decayed with chemical reaction parameter. Srinivasacharya and Shafeeurrahman [8] analysed the flow of a chemically reacting nanofluid for entropy generation analysis with magnetic field and Joule heating effect. It is concluded from the results that the entropy, temperature and velocity of the nanofluid is enhanced by Joule heating parameter, whereas, the velocity is enhanced and the

temperature and entropy generation are depleted by chemical reaction parameter. Masood and Farooq [9] conducted an analysis on thermal stratification and thermal radiation effects due to MHD flow of silver nanoparticles and graphene oxide in water. The inferences of this investigation are that the convective heat transfer decreases with both stratification parameter and radiation parameter. Jha and Samaila [10] examined the impacts of thermal radiation and nonlinear density variation on the MHD flow over an inclined plate. The results show the elevation in heat transfer with angle of inclination and thermal radiation. Oyedepo et al. [11] modelled the thermal performance of alumina nanofluids as coolants in car radiators. Results signified 14% elevation in heat transfer coefficient for 4% increase in volume fraction. Rathore and Sandeep [12] modelled and investigated the blood-based silver and gold nanofluid flow in a stenosed artery with magnetic field and variable heat source effects. This study helps in localized photothermal therapy (PTT) to treat cancer. Algehyne et al. [13] computationally examined the hybrid nanofluid flow due to partially ionized graphene oxide and silver over a stretching sheet. The investigation signifies a decrease in velocity with Hartmann number and an increase with Hall current and ion-slip parameter.

Moreover, many classical and novel methods for numerical and analytical investigations in closed geometries have been widely used. For example, Zeeshan et al. topologically approached the flow of nanofluids using a combined Genetic algorithm and Nelder-Mead method [14] with a conclusion that Dufour number and Dufour-solutal Lewis number enhances Sherwood number while depleting Nusselt number. Kumar et al. [15] explored the study on Powell-Eyring fluid flow in rotating cylinders and found from the results obtained that the velocity profiles increase with rotation and Powell-Eyring parameters. Abro and Abdon [16] investigated fractional Oldroyd-B nanofluid for 1-D flow with ethylene glycol-based molybdenum disulphide, copper, alumina and silver nanoparticles. The conclusions suggest that molybdenum disulphide nanofluid has higher velocity profiles in comparison to the other nanofluids. Studies such as the analysis of squeezing flow of an ionic liquid by Shah et al. [17] with a conclusion that copper nanoparticles among copper, alumina and titania is the best to enhance the heat transfer is worth mentioning. Also, an enhancement in velocity boundary layer is found to be unique to copper nanofluids. A numerical examination of nanofluid flow in a porous annulus is conducted by Miles and Bessaih [18] and entropy and convective heat transfer are observed to increase with the addition of nanoparticles. Jagadeeshwar and Susmitha [19] examined how temperature-dependent viscosity affects graphene nanofluid flow over stretching cylinders using successive linearization method (SLM) and noticed that the mass transport and fluid friction is responsible for generated entropy.

Combining the temperature dependent viscosity studies with cross diffusion effects on nanofluid flow aids in better exploitation of graphene based nanofluids as coolants. Bercovici [20] investigated how current theory is affected by temperature dependent viscosity. Nandy [21] studied to investigate theoretically the flow of viscous stratified fluid over a porous surface and commits to infer fundamental features at length such as the pore size of the medium Barletta and Zanchini [22] analysed the impacts of temperature dependent viscosity of a Newtonian fluid in an inclined channel. The results show that viscosity effects in pressure drops in the presence of buoyancy forces, whereas, regardless of such forces, velocity and friction factors were affected. Sajid et al. [23] examined the impacts of gold nanoparticles under slip conditions on Maxwell velocity and Smoluchowski temperature adapting the Sutterby model. The results indicate that thermal radiation and chemical reaction can boost heat and mass transport by 17.2% and 62.1%, respectively. Harfash and Challoob [24] formulated and used the Brinkman model to study the through-flow in a heterogeneous porous layer with Dufour and Soret effects. This study is significant in microfluidic devices and micro-electro-mechanical systems (MEMS) for analysing the linear and nonlinear stability due to slip

conditions. The influence of variable viscosity and double diffusion on the convective stability of a nanofluid flow in an inclined porous channel is investigated by Humnekar and Srinivasacharya [25]. The results show that increasing the Darcy number, the Lewis number, the Dufour parameter, or the Soret parameter increases the stability of the system, whereas increasing the inclination angle of the channel destabilizes the flow. John et al. [26] investigated the three-dimensional flow of a water-based Ag-MgO hybrid nanofluid in a static cone-disk system while considering temperature-dependent fluid properties. It is found that an increase in the temperature-dependent viscosity parameter enhances heat transfer characteristics in the static cone-disk system, while the thermal conductivity parameter has the opposite effect.

Limited applied and computational studies on graphene nanofluids demands further exploration of their flow. Also, the geometry has extensive industrial applications such as manufacturing of dyes, fertilizers and polymers, space crafts, turbines, atomic plants, missiles, satellites etc. In spite of all the computational investigations in inclined channel, there is lack of literature on the convective study due to graphene oxide nanofluid flow with varying impacts. The goal of the study is to close the gap by examining the graphene oxide nanofluid flow in an inclined channel with slip condition. The obtained numerical solution for the modelled equations are plotted graphically.

2. GOVERNING EQUATIONS

An inclined channel is considered with two parallel plates and it is inclined with an angle α. Graphene oxide nanofluid is considered to flow with pressure ∂p/∂x (constant) and velocity (u, v_0), in the middle of the two plates. The flow is fully developed and the concentration and temperature vary along y. (Refer Figure 1). The boundary layer equations considering, Boussinesq approximation, Brownian motion and thermophoresis are given by [27],

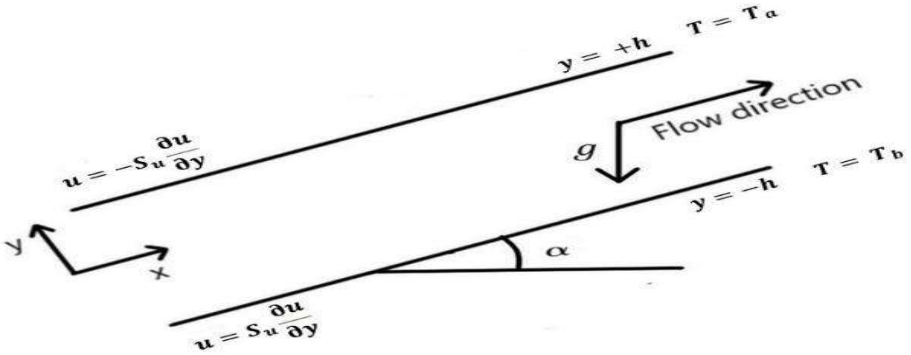

Figure 1. Outline of the flow

$$\frac{\partial u}{\partial x} = 0 \tag{1}$$

$$\rho_{nf} v_0 \frac{\partial u}{\partial y} + \frac{\partial p}{\partial x} = \mu_{nf}\left(\frac{\partial^2 u}{\partial y^2}\right) + \left((1-C_1)(T-T_1)(\rho\beta)_{nf} - (\rho_{sp} - \rho_{bf})(C-C_1)\right) g \sin\alpha \tag{2}$$

$$\frac{\kappa_{nf}}{(\rho C_p)_{nf}}\left(\frac{\partial^2 T}{\partial y^2}\right) + \tau\left(D_B\left(\frac{\partial C}{\partial y}\frac{\partial T}{\partial y}\right) + \frac{D_T}{T_1}\left(\frac{\partial T}{\partial y}\right)^2\right) = 0 \tag{3}$$

$$D_B \frac{\partial^2 C}{\partial y^2} + \frac{D_T}{T_1}\frac{\partial^2 T}{\partial y^2} = 0 \tag{4}$$

along with the following slip boundary conditions [28]

$$\begin{aligned} &at \qquad y=-h,\ u=S_u\frac{\partial u}{\partial y},\ T=T_1,\ C=C_1 \\ &at \qquad y=h,\ u=-S_u\frac{\partial u}{\partial y},\ T=T_2,\ C=C_2 \end{aligned} \tag{5}$$

Here S_u is the length of velocity slip. And C_1, C_2, T_1 and T_2 indicate the concentration and temperature at the bottom and top plates, respectively.
The suffixes *bf*, *sp* and *nf* refer to base fluid, solid particle and nanofluid and the quantities defined below are respectively viscosity, thermal diffusivity, density, specific heat capacity, thermal conductivity, and thermal expansion coefficient [29, 30]. Table 1 displays the thermophysical property values of graphene oxide and water.

$$\begin{aligned} &\mu_{nf}=\frac{\mu_{bf}}{(1-\Phi)^{2.5}},\ \alpha_{nf}=\frac{\kappa_{nf}}{(\rho C_p)_{nf}},\ \rho_{nf}=(1-\Phi)\rho_{bf}+\Phi\rho_{sp},\ (\rho C_p)_{nf}=\Phi(\rho C_p)_{sp}+(1-\Phi)(\rho C_p)_{bf}, \\ &\frac{\kappa_{nf}}{\kappa_{bf}}=\frac{2\Phi(\kappa_{bf}-\kappa_{sp})+\kappa_{sp}+2\kappa_{bf}}{\kappa_{sp}+2\kappa_{bf}-\Phi(\kappa_{bf}-\kappa_{sp})},(\rho\beta)_{nf}=(1-\Phi)(\rho\beta)_{bf}+\Phi(\rho\beta)_{sp} \end{aligned} \tag{6}$$

TABLE 1. Thermophysical properties [31-34]

Property (Units)	**Water**	**GO**
$C_p(J/kgK)$	4179	717
$\sigma(S/m)$	0.005	10^7
$\beta(10^{-5}/K)$	21	28.4
$\kappa(W/mK)$	0.613	5000
$\rho(kg/m^3)$	997.1	1800

The transformation of the equations is achieved through the similarity variables,

$$\eta=\frac{y}{h},\quad u=U_0 f(\eta)\quad \theta(\eta)=\frac{T-T_1}{T_2-T_1},\quad \phi(\eta)=\frac{C-C_1}{C_2-C_1} \tag{7}$$

Thus, the equations (2.1) - (2.5) are transformed as:

$$f''-A_1R_{SC}f'+\frac{Gr}{Re}A_2(A_3\theta-Nr\phi)\sin\alpha^*-A_2P_1=0 \tag{8}$$

$$\theta''+A_4(N_b\theta'\phi'+N_t\theta'^2)=0 \tag{9}$$

$$N_b\phi''+N_t\theta''=0 \tag{10}$$

The boundary conditions are

$$\begin{aligned} &At\ \eta=-1,\quad f-Sf'=0,\quad \theta=0,\quad \phi=0 \\ &at\ \eta=1,\quad f+Sf'=0,\quad \theta=1,\quad \phi=1 \end{aligned} \tag{11}$$

The coefficients in the above equations namely the Reynolds number Re, Grashof number G_r, buoyancy ratio N_r, Brownian motion parameter N_b, thermophoresis parameter N_t, constant pressure gradient P_1, thermal diffusivity α_{bf}, heat capacity ratio τ, Prandtl number Pr and slip parameter S are defined as

$$A_1 = 1-\Phi+\Phi\frac{\rho_{sp}}{\rho_{bf}},\ A_2 = (1-\Phi)^{2.5},\ A_3 = 1-\Phi+\Phi\frac{(\rho\beta)_{sp}}{(\rho\beta)_{bf}},\ A_4 = \left(1-\Phi+\Phi\frac{(\rho C_p)_{sp}}{(\rho C_p)_{bf}}\right),$$

$$Gr = \frac{g\rho_{bf}{}^2\beta_{bf}(1-C_1)(T_2-T_1)h^3}{\mu_{bf}{}^2},\ \mathrm{Re} = \frac{U_0 h}{\nu_{bf}},\ P_1 = \frac{h^2}{U_0\mu_{bf}}\frac{\partial P}{\partial x},\ \alpha = \frac{(\kappa)_{bf}}{(\rho C_p)_{bf}},\ N_b = \frac{\tau D_B(C_2-C_1)}{\alpha}$$

$$N_t = \frac{\tau D_T(T_2-T_1)}{\alpha T_1},\ N_r = \frac{(\rho_{sp}-\rho_{bf})(C_2-C_1)}{(\rho\beta)_{bf}(1-C_1)(T_2-T_1)},\ R_{SC} = \frac{\rho_{bf}v_0 h}{\mu_{bf}},\ S = \frac{S_u}{h},\ \tau = \frac{(\rho C_p)_{sp}}{(\rho C_p)_{nf}}$$

The derived practically important quantities such as local Sherwood number Sh_z and Nusselt number Nu_z, and skin friction C_f are

$$Nu = -\theta'(\pm 1),\ Sh = -\phi'(\pm 1),\ C_f = d_1 f''(\pm 1) \tag{12}$$

where $d_1 = (1-\Phi)^{-2.5}\left((1-\Phi)+\Phi\left(\rho_{sp}/\rho_{bf}\right)\right)^{-1}$. The following section presents the derivation and assessment of entropy number.

3. ENTROPY ANALYSIS

The entropy generation rate [35]

$$S_G = \frac{\kappa_{nf}}{T_1^2}\left(\frac{\partial T}{\partial y}\right)^2 + \frac{\mu_{nf}}{T_1}\left(\frac{\partial u}{\partial y}\right)^2 + RD_B\left(\frac{\partial C}{\partial y}\right)\left(\frac{1}{C_1}\left(\frac{\partial C}{\partial y}\right)+\frac{1}{T_1}\left(\frac{\partial T}{\partial y}\right)\right), \tag{13}$$

is composed of entropy due to concentration, viscous dissipation and temperature. From $S_{G0} = \kappa_{nf}(T_b-T_a)^2/(T_aL)^2$, the characteristic entropy generation rate and S_G, the entropy number is written as $N_S = S_G/S_{G0}$.

On nondimensionalization,

$$\frac{\eta^2}{4}N_S = \frac{1}{\chi}\left(A_6\frac{EcPr}{\Omega_T}f''^2 + \theta'^2 + A_5 M_m\frac{\Omega_C}{\Omega_T}\phi'\left(\frac{\Omega_C}{\Omega_T}\phi'+\theta'\right)\right) \tag{14}$$

$$= N_{S_f} + N_{S_h} + N_{S_G}, \tag{15}$$

where the total entropy is composed of three parts, the entropy number due to fluid friction N_{Sf} and heat transfer N_{Sh} and combined mass and heat transfer N_{SG}. The nondimensional numbers in (3.2) are $c_3 = \kappa_{bf}/\kappa_{nf}$, $c_4 = (1-\Phi)^{-2.5}\,\kappa_{bf}/\kappa_{nf}$, Eckert number $Ec = U_0^2/(\kappa_{bf}C_{pbf}(T_2-T_1))$, constant parameter $\chi = h^2/L^2$, concentration parameter $\Omega_T = C_b/C_a$, combined heat and mass transfer parameter $M_m = RD_BC_0/\kappa_{bf}$ and temperature parameter $\Omega_T = T_b/T_a$.

By estimating Bejan number $Be = N_{Sh}/N_S$ [36], the cause of generated entropy is found. Bejan number, if > 0.5, heat transfer is influences, if < 0.5, combined mass, heat transfer and fluid friction is the major cause and if = 0.5, the three irreversibilities each make an equal contribution [37].

4. NUMERICAL SOLUTION

The equations (2.8) through (2.10) and the related boundary conditions (2.11) are solved using the Spectral quasilinearization method (SQLM) [28, 38, 39]. By expanding the Taylor series about the solution, we linearize the nonlinear variables while ignoring the higher derivatives. Let f_r, θ_r and ϕ_r and f_{r+1}, θ_{r+1} and ϕ_{r+1} be the solutions and improved solutions of the differential equations. Thus, the linearized equations with the boundary conditions are:

$$f''_{r+1} + a_{1,r} f'_{r+1} + a_{2,r}\theta_{r+1} + a_{3,r}\phi_{r+1} = a_{4,r} \tag{16}$$

$$\theta''_{r+1} + b_{1,r}\theta'_{r+1} + b_{2,r}\phi'_{r+1} = b_{3,r} \tag{17}$$

$$c_{1,r}\theta''_{r+1} + \phi''_{r+1} = 0 \tag{18}$$

such that

$$\begin{aligned} &\text{at } \eta = -1, \quad f_{r+1} - Sf'_{r+1} = 0, \quad \theta_{r+1} = \phi_{r+1} = 1 \\ &\text{at } \eta = 1, \quad f_{r+1} + Sf'_{r+1} = 0, \quad \theta_{r+1} = \phi_{r+1} = 0 \end{aligned} \tag{19}$$

The coefficients are given by

$$a_{1,r} = -A_1 R_{SC},\ a_{2,r} = A_2 A_3 \frac{G_r}{R_e}\sin\alpha,\ a_{3,r} = -A_2 \frac{G_r}{R_e} Nr \sin\alpha,\ a_{4,r} = A_2 P_1$$

$$b_{1,r} = A_4 N_b \phi'_r + 2A_4 N_t \theta'_r,\ b_{2,r} = A_4 N_b\ \theta'_r,\ b_{3,r} = A_4 N_b \theta'_r\ \phi'_r + A_4 N_t \theta'^{2}_r,\ c_{1,r} = \frac{N_t}{N_b}$$

Chebyshev polynomials $T_k(\xi) = \cos\left(k\cos^{-1}(\xi)\right)$ are used and f, θ and ϕ are iterated at $\xi_j = \cos(\pi_j/N)$, j = 0, 1, 2, ... N, the Gauss-Lobatto collocation points. Thus, the unknowns and their derivatives are given by

$$f_{r+1}(\xi) \neg \sum_{k=0}^{N} f_{r+1}(\xi_k)T_k(\xi_j),\ \theta_{r+1}(\xi) \neg \sum_{k=0}^{N} \theta_{r+1}(\xi_k)T_k(\xi_j)\ \&\ \phi_{r+1}(\xi) \neg \sum_{k=0}^{N} \phi_{r+1}(\xi_k)T_k(\xi_j) \tag{20}$$

$$\frac{d^r f_{r+1}}{d\eta^r} = \sum_{k=0}^{N} D^r_{kj} f_{r+1}(\xi_k),\ \frac{d^r \theta_{r+1}}{d\eta^r} = \sum_{k=0}^{N} D^r_{kj}\theta_{r+1}(\xi_k)\ \&\ \frac{d^r \phi_{r+1}}{d\eta^r} = \sum_{k=0}^{N} D^r_{kj}\phi_{r+1}(\xi_k),\quad j = 0,1,...N. \tag{21}$$

Here, Chebyshev differentiation matrix is given by $\mathrm{D} = D/2$. Substitution of the above approximations in (4.1) - (4.4) yields,

$$\mathrm{A}\mathrm{Y}_{r+1} = \mathrm{R}_r, \tag{22}$$

with the conditions

$$\begin{aligned} &(1 + SD_{00}) f_{r+1}(\xi_0) + S\sum_{k=1}^{N} D_{0k} f_{r+1}(\xi_k) = 0,\ \theta_{r+1}(\xi_0) = \phi_{r+1}(\xi_0) = 0 \\ &-S\sum_{k=0}^{N-1} D_{Nk} f_{r+1}(\xi_k) + (1 - SD_{NN}) f_{r+1}(\xi_N) = 0,\ \theta_{r+1}(\xi_N) = \phi_{r+1}(\xi_N) = 1 \end{aligned} \tag{23}$$

Initial solutions satisfying (4.4) are chosen as, $f_0 = 0,\ \theta_0 = \phi_0 = (1 - \eta)/2$ and by iterating the equation (4.7) at collocation points, they are numerically solved. In the following section, the results are graphically interpreted.

5. RESULTS

The numerical results of temperature, velocity and concentration are estimated in the section for varied values in the practical range [40, 41]. Parameter values are taken as S = 0.5, Gr = 2×10^5, N_b = 4×10^{-4}, Re = 300, Ec = 10^{-5}, N_r = 2 and N_t = 2×10^{-4}, Pr = 6.5 and Φ = 0.01 unless otherwise stated. SQLM approximation of 100th order is taken to obtain converging results at third iteration and accurate results for specific values for $R_{SC} = A_1 = A_2 = 1$, $Gr = 0$, $P_1 = -1$ and $S = 0$ are obtained [42] (Refer Table 2).

Figure 2 depicts the changes of velocity in line with α, Re, R_{SC} and S. As the angle of inclination is raised, gravitational force strongly impacts the flow of the nanofluid and the velocity decreases (figure 2a). The depictions of figure 2(b) show that, as Re values are raised, effects of viscous forces are lesser, so the fluid moves faster causing *f* profiles to improve. Similarly, figure 2(c) pictures the improvement in velocity, whereas, near the hotter plate, the velocity is slightly greater for the suction parameter in comparison to the case when $R_{SC} = 0$. The depictions of figure 2(d) show that, as S values are raised, the velocity slip is supposed to aid the fluid to move faster overcoming the friction effects thus causing *f* profiles to improve. But with the impacts of gravitational forces, the velocity drops.

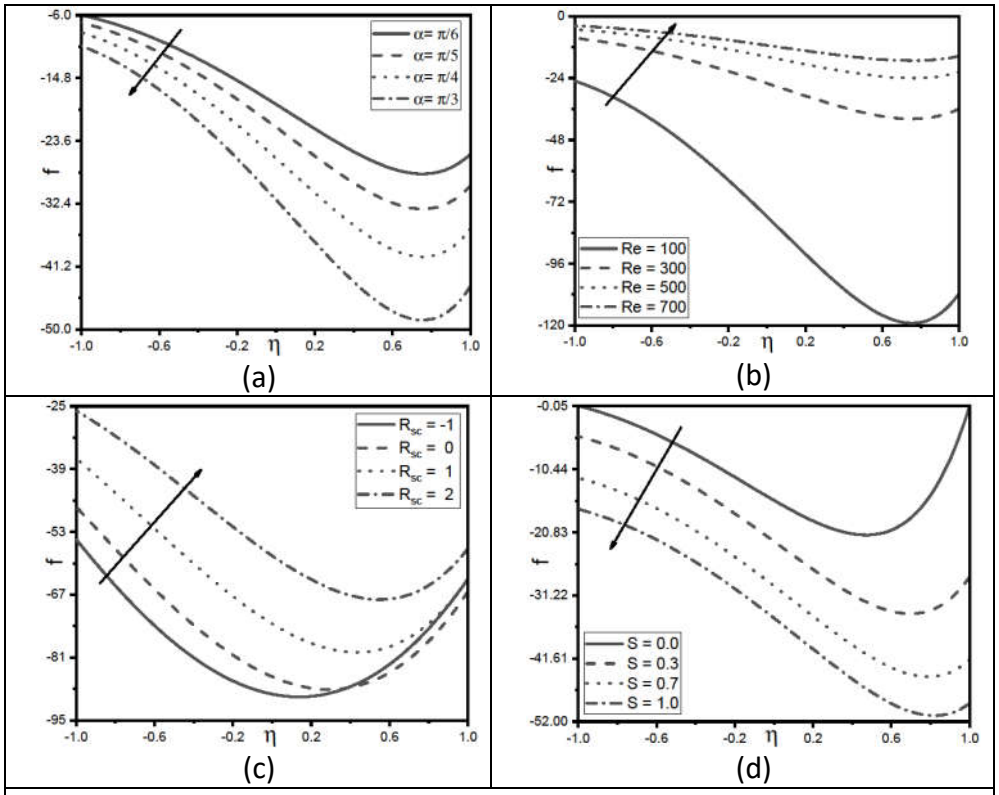

Figure 2. Variations of f in accordance with (a) α, (b) Re, (c) R_{SC} and (d) S

Table 2. f(η) values for $R_{SC} = Ec = 1$, $Pr = 0.71$, $P_1 = -1$, and $D_h = Ha = D_c = 0$ *[40]*

Makinde and Eegunjobi [42]		Present study	
η	f(η)	η	f(η)
1	0	1	0
0.9	0.050545	0.900783	0.050207
0.8	0.086764	0.80021	0.086702
0.7	0.11002	0.700015	0.110017
0.6	0.121546	0.601394	0.121461
0.5	0.122459	0.5	0.122459
0.4	0.113769	0.400145	0.113789
0.3	0.09639	0.299985	0.096387
0.2	0.071149	0.201048	0.071451
0.1	0.038793	0.100158	0.038849
0	0	0	0

The fluctuations of Ns and Be in accordance with α, Re and R_{SC} are shown in the Figure 3. The rises entropy number increases as α value grow. This is because, when angle of inclination is Figure 3 depicts the variations of, increased, the energy is dissipated to aid the fluid flow. Consequently, it causes Be values to decrease throughout the channel (figure 3b). Thus, irreversibility due to fluid friction is responsible for the entropy generated. Whereas, with Re, the entropy generation is decreased, causing Be to deplete throughout the channel (figure 3d). Thus, similar to the previous case, fluid friction contributes to the fall in entropy. Also, The suction parameter increases the entropy value in the vicinity of the surfaces and decreases it throughout the remaining geometry (figure 3e). In contrast, the entropy generation number grows in the middle of the channel and drops at the surfaces for the injection parameter. This in turn has a reverse effect on Be for RSC (figure 3f). Thus, mass transfer contributes to the entropy generation in the case of suction/injection parameter.

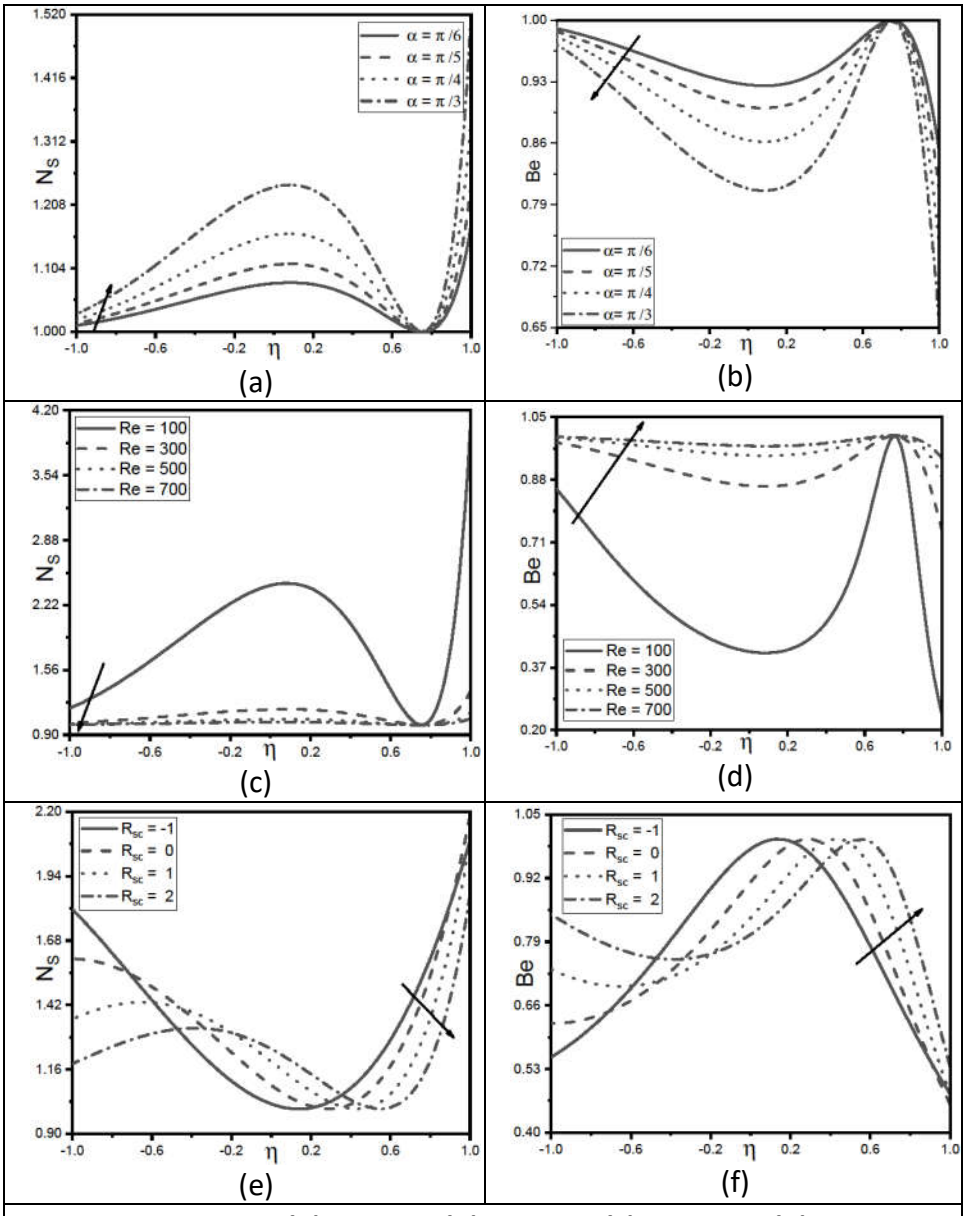

Figure 3. Impacts of (a) α on N_S, (b) α on Be, (c) Re on N_S, (d) Re on Be, (e) R_{SC} on N_S and (f) R_{SC} on Be

Table 3 represents the quantitative data for Cf and Nu at upper plate for different effects. The ratio of qualitative heat transfer from convection to conduction is known as the Nusselt number. Clearly, the increasing values of slip parameter and Reynolds number causes the skin friction to decrease. Whereas, as the angle of inclination increases, skin friction increases. Similarly, when suction/injection parameter increases, skin friction increases. Also, while Nb parameter increases Nu, Sh increases and Skin friction decreases. Consequently, at the wall's surface, Brownian diffusion improves convective heat and mass transport. Likewise, when Nt parameter increases, Nusselt number values increase, whereas, Sherwood and skin friction values decrease. Thus, the convective heat transfer is improved by thermophoretic diffusion. and thermophoretic diffusion of the nanoparticles causing an enhancement in diffusive mass transfer.

TABLE 3: Quantitative data of Nusselt, Sherwood and skin friction

Re	N_b	N_t	R_{SC}	α	S	$-\theta'(1)$	$-\phi'(1)$	$d_1 f'(1)$
100	4	2	5	π/4	0.5	-0.999702	-1.000149	218.689941
300	4	2	5	π/4	0.5	-0.999702	-1.000149	73.140136
500	4	2	5	π/4	0.5	-0.999702	-1.000149	44.030175
700	4	2	5	π/4	0.5	-0.999702	-1.000149	31.554478
300	2	2	5	π/4	0.5	-0.999801	-1.000199	73.140175
300	4	2	5	π/4	0.5	-0.999702	-1.000149	73.140136
300	6	2	5	π/4	0.5	-0.999603	-1.000132	73.138315
300	8	2	5	π/4	0.5	-0.999504	-1.000124	73.136047
300	4	2	5	π/4	0.5	-0.999702	-1.000149	73.140136
300	4	3	5	π/4	0.5	-0.999652	-1.000261	73.132762
300	4	4	5	π/4	0.5	-0.999603	-1.000397	73.124049
300	4	5	5	π/4	0.5	-0.999553	-1.000559	73.114000
300	4	2	-1	π/4	0.5	-0.999702	-1.000149	129.166786
300	4	2	0	π/4	0.5	-0.999702	-1.000149	134.901359
300	4	2	1	π/4	0.5	-0.999702	-1.000149	129.241019
300	4	2	2	π/4	0.5	-0.999702	-1.000149	115.445352
300	4	2	5	π/6	0.5	-0.999702	-1.000149	51.824861
300	4	2	5	π/5	0.5	-0.999702	-1.000149	60.859654
300	4	2	5	π/4	0.5	-0.999702	-1.000149	73.140136
300	4	2	5	π/3	0.5	-0.999702	-1.000149	89.495922
300	4	2	5	π/4	0	-0.999702	-1.000149	215.164948
300	4	2	5	π/4	0.3	-0.999702	-1.000149	95.578878
300	4	2	5	π/4	0.7	-0.999702	-1.000149	60.720359
300	4	2	5	π/4	1	-0.999702	-1.000149	49.879986

6. CONCLUSIONS

Flow of graphene oxide nanofluid in inclined parallel plates is studied and the following are inferred:

- Velocity is enhanced by raising the values of suction parameter, inclination angle and slip parameter.
- For $-1 < \eta < 1$, Be > 0.608. Therefore, heat transfer generates entropy throughout the channel.
- Thermophoresis parameter enhances heat transfer due to convection at the upper plate.

The problem is useful widely ranging from polymer manufacturing, aircraft propulsion system, coolants, automobile radiators, heat exchangers to pharmacotherapy. The study can be extended by analysing non-Newtonian behaviour of the fluid.

References

[1] Özçelik, S. Copper Ferrite Nanoparticles: Structural, Magnetic, Optical, Photocatalytic Activity and Blood Compatibility Properties. *BioNanoScience*, 1-15, (2023). Doi: 10.1007/s12668-023-01130-0
[2] Alam, J., Murtaza, M. G., Tzirtzilakis, E. E., and Ferdows, M. A Parametric Simulation of MHD Flow and Heat Transfer of Blood-Fe3O4 Over an Exponentially Stretching Cylinder. *BioNanoScience*, 13(3), 891-899, (2023). Doi: 10.1007/s12668-023-01141-x.
[3] Alicanoğlu, P., Ulusoy, Ç., and Sponza, D. Effect of Graphene-TiO2 on the photodegradation of olive mill effluent and recovery of Graphene-TiO2. *Sigma Journal of Engineering and Natural Sciences*, 8(3), 227-234, (2017).
[4] Akçağlar, S. Separation of Co (ii) and Se (vi) from a metal and glass industry wastes using graphene oxide-mangane oxide nanocomposite. *Sigma Journal of Engineering and Natural Sciences*, 38(1), 29-46, (2020).
[5] Akkaya, E., and Çavdar, U. Investigation of sintering conditions and the gnp additions on aluminum compacts. *Sigma Journal of Engineering and Natural Sciences*, 38(4), 1977-1986, (2020).
[6] Ergüner, A., Özkan, R., Kemal, K. O. C. A., and Genc, M. S. Improvement of mechanical behaviour of wind turbine blade using nanofluid graphene and/or glass fiber in epoxy resin. *Sigma Journal of Engineering and Natural Sciences*, 39(1), 58-69, (2021).
[7] Srinivasacharya, D. and Shiferaw, M. Cross diffusion effects on chemically reacting magnetohydrodynamic micropolar fluid between concentric cylinders. *Journal of heat transfer*, 135(12), 122003, (2013). Doi: 10.1115/1.4024838
[8] Srinivasacharya, D. and Shafeeurrahman, M. Joule heating effect on entropy generation in MHD mixed convection flow of chemically reacting nanofluid between two concentric cylinders. *International Journal of Heat and Technology*, 35(3), 487-497, (2017). Doi: 10.18280/ijht.350305
[9] Masood, S. and Farooq, M. Influence of thermal stratification and thermal radiation on graphene oxide-Ag/H2O hybrid nanofluid. *Journal of Thermal Analysis and Calorimetry*, 143(2), 1361-1370, (2021). Doi: 10.1007/s10973-020-10227-7
[10] Jha, B. K. and Samaila, G. Nonlinear approximation for buoyancy-driven mixed convection heat and mass transfer flow over an inclined porous plate with Joule heating, nonlinear thermal radiation, viscous dissipation and thermophoresis effects. *Numerical Heat Transfer, Part B: Fundamentals*, (2022). Doi: 10.1080/10407790.2022.2150341
[11] Oyedepo, S. O. et al. Numerical modeling of heat transfer performance and optimization of car radiator using (H2O/Al2O3) nanofluids as coolant. *Numerical Heat Transfer, Part B: Fundamentals*, 82(5), 185-198, (2022). Doi: 10.1080/10407790.2022.2083854
[12] Rathore, N. and Sandeep, N. Computational framework on heat diffusion in blood-based hybrid nanoliquid flow through a stenosed artery: An aligned magnetic field application. *Numerical Heat Transfer, Part B: Fundamentals*, (2022). Doi: 10.1080/10407790.2022.2153768
[13] Algehyne, E. et al. Analysis of the MHD partially ionized GO-Ag/water and GO-Ag/kerosene oil hybrid nanofluids flow over a stretching surface with Cattaneo-Christov double diffusion. *International Communications in Heat and Mass Transfer*, 136, 106205, (2022).
[14] Zeeshan, A. et al. Flow of Viscous Nanofluid Between the Concentric Cylinders, *Journal of Computational and Theoretical Nanoscience*, 11(3), 646-654, (2014). Doi: 10.1166/jctn.2014.3408
[15] Kumar, D., Ramesh, K. and Chandok, S. Mathematical modeling and simulation for the flow of magneto-Powell-Eyring fluid in an annulus with concentric rotating cylinders, *Chinese Journal of Physics*, 65, 187-197, (2020). Doi: 10.1016/j.cjph.2020.02.002
[16] Abro, K. A. and Abdon, A. A computational technique for thermal analysis in coaxial cylinder of one-dimensional flow of fractional Oldroyd-B nanofluid. *International Journal of Ambient Energy*, 43(1), 5357-5365, (2022). Doi: 10.1080/01430750.2021.1939157
[17] Shah, R. A. et al. Parametric analysis of the heat transfer behavior of the nano-particle ionic-liquid flow between concentric cylinders. *Advances in Mechanical Engineering*, 13(6), 168781402110240, (2021). Doi: 10.1177/16878140211024009
[18] Miles, A. and Bessaih, R. Heat transfer and entropy generation analysis of three-dimensional nanofluids flow in a cylindrical annulus filled with porous media. *International Communications in Heat and Mass Transfer*, 124, 105240, (2021). Doi: 10.1016/j.icheatmasstransfer.2021.105240

[19] Pashikanti, J. and Susmitha Priyadharshini, D. R. Influence of Variable Viscosity on Entropy Generation Analysis Due to Graphene Oxide Nanofluid Flow. *Journal of Nanofluids*, 12(5), 1360-1373, (2023). Doi: 10.1166/jon.2023.2026
[20] Bercovici, D. A theoretical model of cooling viscous gravity currents with temperature-dependent viscosity. *Geophysical research letters*, 21(12), 1177-1180, (1994). Doi: 10.1029/94GL01124
[21] Nandy, K. C. Study of the viscous flow over a porous boundary (Doctoral dissertation, University of North Bengal), (1995).
[22] Barletta, A. and Zanchini, E. Mixed convection with variable viscosity in an inclined channel with prescribed wall temperatures. *International Communications in Heat and Mass transfer*, 28(8), 1043-1052, (2001). Doi: 10.1016/S0735-1933(01)00308-6
[23] Sajid, T., Jamshed, W., Shahzad, F., Akgül, E. K., Nisar, K. S. and Eid, M. R. Impact of gold nanoparticles along with Maxwell velocity and Smoluchowski temperature slip boundary conditions on fluid flow: Sutterby model. *Chinese Journal of Physics*, 77, 1387-1404, (2022). Doi: 10.1016/j.cjph.2021.11.011
[24] Harfash, A. J. and Challoob, H. A. Slip boundary conditions and through flow effects on double-diffusive convection in internally heated heterogeneous Brinkman porous media, *Chinese Journal of Physics*, 56(1), 10-22, (2018). Doi: 10.1016/j.cjph.2017.11.023
[25] Humnekar, N., Srinivasacharya, D. Influence of variable viscosity and double diffusion on the convective stability of a nanofluid flow in an inclined porous channel. *Applied Mathematics and Mecha*nics, 45, 563–580, (2024). https://doi.org/10.1007/s10483-024-3096-6
[26] John, A.S., Mahanthesh, B. & Lorenzini, G. Study of hybrid nanofluid flow in a stationary cone-disk system with temperature-dependent fluid properties. *Applied Mathematics and Mecha*nics, 45, 677–694, (2024). https://doi.org/10.1007/s10483-024-3089-5
[27] Buongiorno, J. Convective Transport in Nanofluids. *Journal of Heat Transfer*, 128(3), 240-250, (2006). Doi: 10.1115/1.2150834
[28] Srinivasacharya, D. and Hima Bindu, K. Entropy generation in a micropolar fluid flow through an inclined channel with slip and convective boundary conditions. *Energy*, 91, 72-83, (2015). Doi: 10.1016/j.energy.2015.08.014
[29] Ghadikolaei, S. S. et al. Investigation for squeezing flow of ethylene glycol (C2H6O2) carbon nanotubes (CNTs) in rotating stretching channel with nonlinear thermal radiation. *Journal of Molecular Liquids*, 263, 10-21, (2018). Doi: 10.1016/j.molliq.2018.04.141
[30] Chu, Y.-M. et al. Mixed Convection in MHD Water-Based Molybdenum Disulfide-Graphene Oxide Hybrid Nanofluid through an Upright Cylinder with Shape Factor. *Water*, 12(6), 1723, (2020). Doi: 10.3390/w12061723
[31] Lide, D. R. and Kehiaian, H. V. CRC HANDBOOK of THERMOPHYSICAL and THERMOCHEMICAL DATA, CRC HANDBOOK of THERMOPHYSICAL and THERMOCHEMICAL DATA. CRC Press, (2020). Doi: 10.1201/9781003067719
[32] Al-Sankoor, K. et al. Analytically investigating of heat transfer parameters with presence of graphene oxide nanoparticles in Williamson-magnetic fluid by AGM and HPM methods. *Case Studies in Thermal Engineering*, 27, 101236, (2021). Doi: 10.1016/j.csite.2021.101236
[33] Gul, T. et al. Thermal Performance of the Graphene Oxide Nanofluids Flow in an Upright Channel Through a Permeable Medium. *IEEE Access*, 7, 102345-102355, (2019). Doi: 10.1109/ACCESS.2019.2927787
[34] Elsaid, K. et al. Thermophysical properties of graphene-based nanofluids. *International Journal of Thermofluids.* 10, 100073, (2021).
[35] Bejan, A. Entropy generation minimization: The new thermodynamics of finite-size devices and finite-time processes. *Journal of Applied Physics*, 79(3), 1191-1218, (1996). Doi: 10.1063/1.362674.
[36] Bejan, A. and Kestin, J. Entropy Generation Through Heat and Fluid Flow. *Journal of Applied Mechanics*, 50(2), 475-475, (1983). Doi: 10.1115/1.3167072
[37] Paoletti, S., Rispoli, F. and Sciubba, E. Calculation of exergetic losses in compact heat exchanger passages. *in ASME AES*, 21-29, (1989)
[38] Bellman, R. E. and Kalaba, R. E. Quasilinearization and Nonlinear Boundary-Value Problems. *The American Mathematical Monthly*, 74(9), 1157, (1967). Doi: 10.2307/2313669
[39] Canuto, C. et al. Spectral Methods, Berlin, Heidelberg: Springer Berlin Heidelberg (Scientific Computation), (2006). Doi: 10.1007/978-3-540-30726-6
[40] Malashetty, M. S., Umavathi, J. C. and Prathap Kumar, J. Convective magnetohydrodynamic two fluid flow and heat transfer in an inclined channel. *Heat and Mass Transfer*, 37(2-3), 259-264, (2001). Doi: 10.1007/s002310000134
[41] Behseresht, A., Noghrehabadi, A. and Ghalambaz, M. Natural-convection heat and mass transfer from a vertical cone in porous media filled with nanofluids using the practical ranges of nanofluids thermo-physical

properties. *Chemical Engineering Research and Design*, 92(3), 447-452, (2014). Doi: 10.1016/j.cherd.2013.08.028
[42] Makinde, O. D. and Eegunjobi, A. S. Effects of convective heating on entropy generation rate in a channel with permeable walls. *Entropy*, 15(1), 220-233, (2013). Doi: 10.3390/e15010220